Assessment of performance characteristics of photoswitchable bacteriophytochromes at different depths using optoacoustic mesoscopy

LUDWIG ENGLERT,[1,2] (ID) BJARNE PERLEBERG,[1,2] SHILPA TAYAL,[1,2] BINGZHI WANG,[1,2] YISHU HUANG,[1,2] AZEEM MOHAMMED,[1,2] HAILONG HE,[1,2] ANDRE C. STIEL,[2,3] AND VASILIS NTZIACHRISTOS[1,2,4,*] (ID)

[1] *Chair of Biological Imaging, Central Institute for Translational Cancer Research (TranslaTUM), School of Medicine and Health & School of Computation, Information and Technology, Technical University of Munich, Munich, Germany*
[2] *Institute of Biological and Medical Imaging, Bioengineering Center, Helmholtz Zentrum München, Neuherberg, Germany*
[3] *Protein Engineering for Superresolution Microscopy Lab, Institute for Biophysics and Physical Biochemistry, University of Regensburg, Regensburg, Germany*
[4] *Munich Institute of Biomedical Engineering (MIBE), Technical University of Munich, Garching b. München, Germany*
[*]bioimaging.translatum@tum.de

Abstract: Photoswitchable proteins have so far been barely investigated in the field of optoacoustic (OptA) mesoscopy. In particular, the unmixing performance and achievable depth with photoswitchable bacteriophytochromes in an OptA mesoscopy setup with a single-element detector remain uncharted. Therefore, this study investigates the switching kinetics and unmixing performance at two wavelengths of photoswitchable bacteriophytochromes expressed by *E. coli* cells in an OptA mesoscopy set up with a single-element spherically focused 25 MHz piezoelectric detector at different depths using a light scattering phantom. We found that the signal-to-noise ratio dropped by approximately 5 dB/mm as a consequence of declining detector sensitivity, attenuation of the acoustic wave, and decreasing fluence. This limited unmixing with the current system parameters to a depth of 2-4 millimeters. The analysis of the switching kinetics indicates that an increased number of laser pulses was needed to switch the protein between the ON- and OFF states as depth increases. Based on these analyzed switching kinetics, recommendations can be made regarding the pulsing schemes needed at different depths. The knowledge gained on the required pulsing schemes for successful protein switching, unmixing performance, and achievable depth can be leveraged in future ex-vivo/in-vivo studies using photoswitchable proteins combined with OptA mesoscopy.

1. Introduction

Optoacoustic (OptA) imaging, succinctly described as "light in, sound out", is a novel emerging imaging technology that combines the benefits of optical and acoustic imaging. OptA imaging leverages on non-radiative relaxation which results in a minute temperature increase in chromophore-containing volumes, leading to the volumetric expansion and contraction that gives rise to ultrasound waves. These ultrasound waves can be detected and used to reconstruct the optical contrast. Compared to purely optical methods, OptA imaging achieves higher resolution deep in tissues, i.e. deeper than the depths reached with optical microscopy due to reduced

scattering and attenuation of acoustic waves. This innovative approach is beginning to make a considerable impact in the field of biomedical science [1–4]. Originally introduced as a molecular imaging technology, OptA has undergone considerable advancements, also driven by the development of OptA contrast agents and reporter genes. These developments enable visualization of different structures in a manner similar to fluorescent labels in optical imaging. However, unlike optical microscopy, the background signals from endogenous chromophores, such as melanin, hemoglobin, are relatively strong in OptA, which hinders the spectral separation of different chromophores [5]. A new source of contrast that could overcome these limitations are photoswitchable proteins. Photoswitchable proteins are light-sensitive molecules that can reversibly change their structure or optical properties in response to light of specific wavelengths [5]. As such, the separation between different chromophores is switched from the spectral domain to the time domain, which has been shown to provide improved image contrast by enabling identification and subtraction of background signals, leading to enhanced specificity as well as sensitivity [5–8]. The use of photoswitchable proteins in OptA tomography in the macroscopic domain is a relatively recent development, providing resolutions of up to 100 μm [1,5,8,9]. However, few studies have examined the use of photoswitchable proteins in the mesoscopic regime, and none have characterized the switching kinetics and unmixing performance over depth for single-element detector systems. As a result, the high resolution offered by such systems, on the order of tens of micrometers [9–11], cannot currently be exploited. Furthermore, the potential benefits of applying photoswitchable proteins in single-element detector OptA mesoscopy, particularly in terms of its performance at different depths, remains unclear. Single-element detector system designs have been shown to provide higher resolution and greater sensitivity compared to multi-element detector systems [9,12,13]. Additionally, they feature lower electromechanical complexity by requiring only a single data acquisition channel, which contributes to reduced overall system costs [14]. The knowledge on the performance at difference depth could be leveraged in future ex-vivo/in-vivo studies to fully exploit the advantages of using photoswitchable proteins in the mesoscopic regime with single-element detector implementations.

The usage of photoswitchable proteins in the macroscopic and mesoscopic OptA imaging domains has been investigated in multiple studies so far [7,11,15–18]. Commonly used photoswitchable proteins include bacteriophytochromes (BphP), which exhibit absorption peaks in the near-infrared range above 700 nm. This represents a considerable red-shift compared to GFP-like photoswitchable proteins (<650 nm), enabling BphPs to exhibit improved performance due to higher tissue penetration and lower background interference at these wavelengths [19]. Moreover, unlike other phytochromes, BphPs utilize biliverdin as their chromophore. Biliverdin, a byproduct of heme catabolism, is readily available in most mammalian cells, enabling BphPs to function as fully genetically encoded reporters. Additionally, BphPs exhibit a relatively high molar absorptivity ($\sim$100,000 $M^{-1}\,cm^{-1}$), while having a low fluorescence quantum yield. This results in substantial non-radiative relaxation, thereby generating strong OptA signals. BphPs have been used in combination with an OptA macroscopic tomography setup based on a full-ring ultrasonic transducer array with a 5 MHz center frequency to visualize tumor growth and metastasis at a depth approaching 10 mm [7]. Additionally, the switching ratios based on differential signals were also analyzed in a scattering phantom at a depth of 10 mm. In a similar study using a slightly modified setup, RpBphP1, and a novel bacteriophytochrome DrBphP-PCM, as well as a split version of DrBphP-PCM, were used for deep tumor in-vivo imaging in the liver and kidney [15]. Additionally, switching ratios based on temporal frequency lock-in analysis have been evaluated at depths of 0 and 12 mm in a scattering phantom. The BphPs, DrBphP-PCM and ReBphP1-PCM, have also been utilized for the imaging of T lymphocytes, bacteria, and tumors in-vivo in the mouse body and brain at depths of up to 10 mm [18]. This was achieved using a commercially available OptA macroscopic tomography setup with a 256-element transducer array at a center frequency of 5 MHz. However, the systems mentioned above operate in the

macroscopic OptA domain with a multi-element detector, and hence, the acquired data cannot be extended to single-element focused piezoelectric detector OptA mesoscopy.

In the mesoscopic OptA regime, photoswitchable proteins have also been applied for background suppression in tumor monitoring in living mice, and in a scattering phantom at depths of up to 10 mm [16]. This study was performed using a setup with a 15 MHz 128-element ultrasound linear array transducer. In another study, capitalizing on a commercial OptA mesoscopy setup equipped with a 256-element transducer array (25 to 55 MHz), a photoswitchable bacteriophytochrome (DrBphP-CBD) was employed for the in-vivo imaging of tumors in mice. The imaging depth, as well as the switching cycles and the switching ratios of the differential signals, have been investigated in chicken breast at depths of 0 and 10 mm. Although both setups mentioned above operate in the mesoscopic domain, they use multi-element detectors. As such, the data presented cannot be directly applied to scenarios where single-element detector systems are used.

A single-element detector equivalent OptA mesoscopic setup based on an all optical Fabry Pérot polymer film ultrasound detector (19-39 MHz) has also been reported for tumor imaging of AGP1, a photoswitchable phytochrome-based reporter protein [11]. This setup enabled longitudinal deep in-vivo imaging. However, this study lacks characterization of the switching kinetics, achievable signal-to-noise (SNR), and unmixing performance at different depths. Moreover, the sensitivity and the sensitivity field characteristics between planar Fabry Pérot detectors and focused piezoelectric detectors may differ.

In summary, numerous studies have already shown the advantages of photoswitchable proteins in OptA imaging. However, the investigations were mostly performed using multi-element transducer arrays in the macroscopic or mesoscopic regime or they lacked a detailed analysis of the SNR, unmixing performance, and switching kinetics at different depths for single-element piezoelectric detectors. Moreover, all studies have in common to focus mainly on the switching aspects for a single wavelength, while the switching kinetics for the second wavelength used for switching back the protein are not considered.

As demonstrated in various other OptA implementations, we hypothesize that the SNR, switching kinetics, and unmixing performance of photoswitchable BphPs will vary at different depths when using a single-element focused piezoelectric detector mesoscopic OptA setup. We evaluated these parameters for two photoswitchable BphPs, specifically ReBphP-PCM and DrBphP-PCM. Sets of three tubings filled with *E. coli* expressing either ReBphP-PCM or DrBphP-PCM, as well as defibrinated horse blood, were integrated into a scattering phantom to enable measurements at different depths. These measurements were collected using a single detector element OptA mesoscopy setup at two different wavelengths. ReBphP-PCM and DrBphP-PCM were chosen as they pose the two opposing extremes in terms of switching kinetics among the available BphPs with ReBph-PCM switching roughly 4 times faster than DrBphP-PCM. Based on the characterized switching kinetics, we found that the number of pulses needed to switch the proteins between the ON- and OFF-states must be increased with depth by a factor of approximately two over 4 mm and largely differs for the analysed wavelength. Furthermore, we found an SNR drop of approximately 5 dB per mm, which resulted from the declining sensitivity of the detector, attenuation of the acoustic wave, and dropping fluence due to scattering and beam divergence. As a result, successful unmixing could be achieved at depths of 2-4 mm for the current setup. In summary, our experiments reveal the switching kinetics and unmixing performance at different depths and different wavelength for photoswitchable proteins in single-element detector OptA mesoscopy.

2. Methods

2.1. OptA mesoscopy setup

A custom OptA mesoscopy setup (see Fig. 1(a)) was developed to characterize the SNR, the switching kinetics and contrast-to-background ratio from two different photoswitchable BphPs

expressed by *E. Coli* at different depths (see Fig. 1(b)). The setup was based on a tuneable nanosecond laser (DPSS 250 OPO) with a 50 Hz repetition rate and a wavelength range of 420-2400 nm (Innolas, Krailing, Germany). The initially high laser output energy of 3 mJ was reduced to approximately 350 µJ using a neutral density filter to avoid exceeding the damage threshold of the optical fiber. The system was configured to operate at 680 and 770 nm, which poses a balance between the available optics, the laser properties and the absorption peaks of the two proteins, ReBphP-PCM and DrBphP-PCM. In order to illuminate the photoswitchable proteins with 680 or 770 nm light to switch between ON- and OFF-states, the beam was separated into its horizontal component (signal) and vertical component (idler) via a polarizing beam splitter (PBS) and guided through a 680/10 nm and 770/10 nm bandpass filters (Thorlabs, GmbH, Bergkirchen, Germany), respectively. The filtered beams were then combined using another PBS and guided via a fiber coupler with a 50 mm focal length plano-convex lens (Thorlabs, GmbH, Bergkirchen, Germany) into a 200 µm multimode fiber with a numerical aperture (NA) of 0.39 (Thorlabs, GmbH, Bergkirchen, Germany). The other end of the fiber was inserted in a through hole spherically focused 25 MHz piezo composite transducer with a focal distance of 4 mm (Sonaxis, Besacon, FR). The pulse energies were measured at 150 µJ per pulse with 9% fluctuations at 680 nm and 270 µJ with 15% fluctuations at 770 nm. All OptA signals and the subsequently derived parameters were rescaled according to the mean pulse energy difference between the 680 and 770 nm pulses. The OptA signals were digitalized with a 1 Gs/s 700 MHz data acquisition card (Gage, Lockport, USA) and analyzed using MATLAB. Sample alignment was performed with a manual x-, y- and z-stage.

2.2. Protein expression

E. coli (strain BL21 (DE3), #C2527, New England Biolabs, Ipswich, USA) were transfected with plasmids expressing ReBphP-PCM or DrBphP-PCM using standard electroporation protocols. Transformed cells were spread on LB agar plates containing 100 µg/mL ampicillin and 15 µM IPTG. The plates were then incubated at 22 °C for 60-66 hours to allow colony formation. *E. coli* were found to exhibit a lower expression of ReBphP-PCM compared to DrBphP-PCM in this setting. After harvesting, the cells were diluted 1:1 with phosphate-buffered saline to facilitate filling of the tubings with a homogenous cell suspension.

2.3. Phantom

The 3D-printed phantom scaffold presented in Fig. 1(b) resembled the shape of a "U" with 1 mm steps going up the arms of the U towards the base of the U. Three tubings with diameters of 200 µm (Smith medical Portex, USA) were fixed across stairs of the same height. The first tubing was filled with DrBphP-PCM expressing *E. coli*, the second with defibrinated horse blood (Thermo Fisher Diagnostics, USA), and the third with ReBphP-PCM expressing *E. coli*. The blood-filled tubing was added to demonstrate unmixing from an endogenous chromophore and to act as a control for the drop in SNR over depth. The set of 3 tubings on the highest step, which was defined as 0 mm depth, were placed sequentially in the acoustic focus, i.e., 4 mm from the detector's surface. For each consecutive step measured on the phantom, the distance between the tubings and the acoustic detector increases by ≈1 mm. The entire phantom was submerged in a scattering medium (water with 0.5% intralipid). The scattering medium also served as the coupling medium.

2.4. Data acquisition and processing

The OptA signals were detected while illuminating each tubing at various depths with light at either 680 nm or 770 nm. Switching between a photoswitchable protein's ON- and OFF-states constitutes one switching cycle. To determine the number of pulses needed to achieve switching at different depths, we applied 100 pulses at 680 nm followed by 100 pulses at 770 nm,
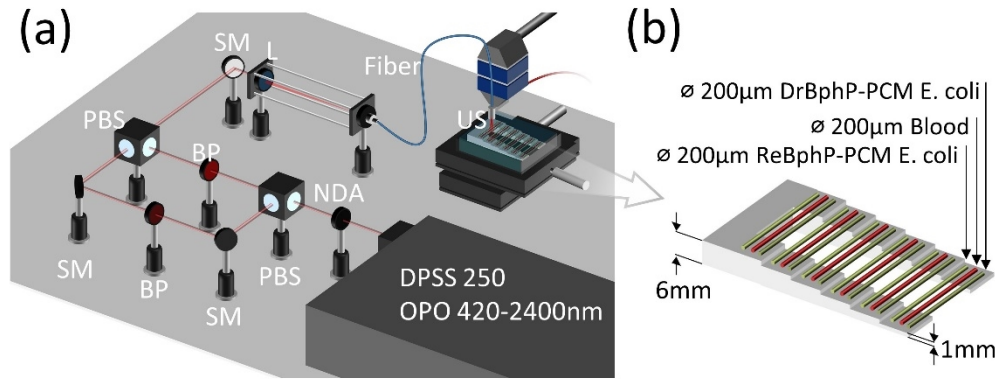
Fig. 1. Schematic illustration of the optoacoustic (OptA) mesoscopy setup and the phantom for the characterization of photoswitchable bacteriophytochromes (BphPs) at different depths. a) The OptA setup is employed in sensing mode. The system utilizes an optical parametric oscillator (OPO), which provides nanosecond light pulses between 420 and 2400 nm. The output beam is attenuated with a neutral density absorption filter (NDA) and separated via a polarizing beam splitter (PBS) into a signal and an idler beam to isolate either 680 or 770 nm beams using band pass (BP) filters. These two beams are then recombined via a PBS before coupling them into a fiber using a 50 mm focal length plano-convex lens (L) to provide illumination to the sample that alternates periodically between 680 and 770 nm. The generated OptA signals are then detected by a 25 MHz spherically focused single-element piezoelectric transducer (US). b). The phantom for the characterization of photoswitchable BphPs at different depths consists of a U-shaped frame with steps (∼10 × 10 mm lateral and axial size of the step) going up the parallel sides at 1 mm increments towards the base of the U. Three tubings (200 μm inner diameter) are fixed across steps of the same height and two of these tubings contain photoswitchable proteins (1x DrBphP-PCM or 1x ReBphP-PCM) expressing *E. coli* and one tubing contains 1x defibrinated horse blood. The tubings on the top step were considered to be at 0 mm depth. The transducer of the OptA mesoscopy setup is placed above the center of each tubing to record the OptA signals emitted. Silver Mirror (SM).

ensuring successful switching. Our results were averaged over 100 switching cycles, based on previous publications [20,7,11], to achieve an optimal balance between SNR improvement and measurement time, resulting in a SNR enhancement of ≈20 dB. The residual standard deviation in the switching curves was estimated from the standard deviation prior to averaging, which was subsequently adjusted by a factor of 10 to account for averaging. This error estimation was validated by comparing the standard deviation across 100 pulses of the blood switching curves at 680 nm or 770 nm excitation before and after averaging, which showed a reduction in standard deviation by a factor of 9.3–9.8 across all depths, confirming consistent performance of the estimation of the remaining standard deviation.

The analysis of the resulting 200 A-lines for each sample involved band pass filtering (1 to 50 MHz) and extracting the OptA signal's peak-to-peak (P2P) amplitude. The time point corresponding to the positive peak of the OptA signal was used to calculate the precise distance between the acoustic focus and the tubing at each measurement step. These corrected distance values were then used for all subsequent analyses. The switching kinetics were evaluated using an exponential function of the form:

$$f(x) = a \cdot e^{-\frac{x}{\tau}} + c$$

Curve fitting using this exponential model was performed employing the Nonlinear Least Squares Methods with time constants (τ) determined individually for each tubing, which may be

positioned at varying depths and contain different samples. Fitted parameters (τ) corresponding to a goodness of fit (R^2) below 0.8 were excluded from further analysis. This threshold represents an experimentally determined balance between ensuring a good model agreement and minimizing the exclusion of data points from subsequent analysis. For the assessment of the unmixing performance a contrast-to-background ratio (CBR) has been defined as

$$CBR := \frac{norm.\ DynR_{Protein}}{norm.\ DynR_{Blood}}$$

where the normalized dynamic range (norm. DynR) is defined as the ON-state value minus the OFF-state value, divided by the mean signal amplitude. In other words, it is the difference between the OptA signal amplitude of the last pulse and the OptA signal amplitude of the first pulse, divided by the mean signal amplitude of all pulses. This normalization approach has been chosen to account for the varying expression levels of the photoswitchable proteins by the bacterial cultures.

3. Results

3.1. OptA signals and switching curves for 680 and 770 nm

In a first step we assessed the OptA A-lines at different depth for DrBphP-PCM- or ReBphP-PCM-expressing *E. coli* and blood acquired from tubings in different depths, whereby each A-line is averaged over all recordings of the same wavelength (5,000 pulses) for the plots in Fig. 2(a) and (b). The depth of 0 mm refers to a measurement at the acoustic focus. As depth increases from the acoustic focus, the signal amplitude drops while the time-of-flight increases, depending on the actual distance between the detector and tubing. Figure 2(c) shows the OptA P2P signal amplitude over 200 pulses for DrBphP-PCM- or ReBphP-PCM-expressing bacteria and blood. The first 100 pulses were delivered at 680 nm, followed by the next 100 pulses at 770 nm. A pulse train at 680 nm and a pulse train at 770 nm together constitute one switching cycle whereby each plot in Fig. 2(c) represents the average over 100 cycles. The curves show an exponential decay of the OptA signal intensity for DrBphP-PCM expressing cells and ReBphP-PCM expressing cells, while blood shows essentially a line that is only affected by noise. The large difference in amplitude between the 680 nm excitation and 770 nm excitation can be attributed to the different extinction coefficients which is higher for 680 nm compared to 770 nm in the DrBphP-PCM and ReBphP-PCM expressing cells and lower for 680 nm compared to 770 nm in blood.

3.2. Signal-to-noise ratio and dynamic range

As a next step based on the presented switching curves we investigated the development of the SNR and the DynR over depth (see Fig. 3). For these graphs the solid line with diamonds shows the maximum SNR and the dashed line with asterisk shows the minimum SNR. The maximum and minimum SNR also represent the ON- and OFF-state for the two bacteria cultures expressing DrBphP-PCM and ReBphP-PCM while for blood these two values represent the noise and fluctuations of the blood OptA signal. The general level of the ON-set SNR for DrBphP-PCM expressing *E. coli* is higher compared to ReBphP-PCM expressing *E. coli* due to a higher protein expression as ReBphP-PCM is even expected to have a higher extinction coefficient and OptA quantum yield compared to DrBphP-PCM. Nevertheless, the ON-state SNR plots allow to assess the drop of the SNR over depth for both bacteria cultures which is approximately 20 dB over 4 mm or 5 db/mm which is further supported by the maximum SNR of the blood signal. However, for both bacteria cultures the drop at 770 nm is slightly lower and has been quantified with approximately 3.5 dB/mm. The OFF-set SNR mostly follows the same trend as the ON-state SNR as both undergo the same signal attenuation. The distance between the ON-state SNR and OFF-state SNR allows to directly assess and compare the relative DynR
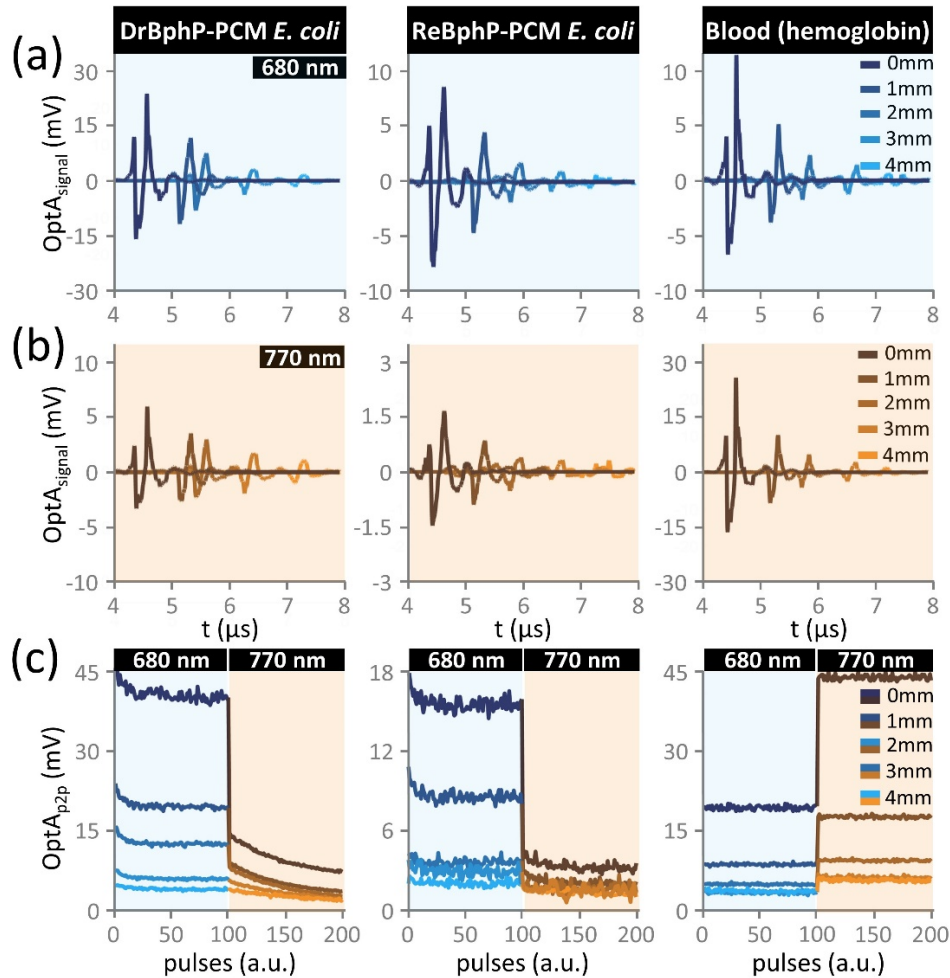
Fig. 2. Detected optoacoustic signals (OptA$_{signal}$) and switching curves (OptA$_{p2p}$) for two photoswitchable bacteriophytochromes (DrBphP-PCM or ReBphP-PCM) expressed by *E. coli* and blood at different depths (see phantom in Fig. 1(b)). a) Averaged OptA signals of DrBphP-PCM- or ReBphP-PCM-expressing *E. coli* and blood at different depths for 680 nm excitation. b) Averaged OptA signals of DrBphP-PCM- or ReBphP-PCM-expressing *E. coli* and blood at different depths for 770 nm excitation. c) OptA switching curves for DrBphP-PCM- or ReBphP-PCM-expressing *E. coli* and blood averaged over 100 switching cycles after 680 nm (in blue tones) and 770 nm (in orange tones) excitation at different depths.

between the two states which has been found to be 20% for cells expressing DrBphP-PCM at 680 nm and 22% for ReBphP-PCM expressing cells. At 770 nm the relative DynR for DrBphP-PCM cells has been quantified with 62% and 46% for ReBphP-PCM cells, both larger than for 680 nm, indicating a larger DynR at 770 nm. At greater depths, the differential value counterintuitively increases, which can be attributed to noise. More specifically, for smaller signal amplitudes noise increasingly influences the assessment of the highest and lowest SNR values, thereby increasing the apparent difference between the maximum and minimum SNR. For the differentiation of multiple chromophores based on their differential value, this value must exceed the system noise, which is particularly present in the remaining variation of the blood signal that does not undergo

any kind of switching. In other words, because the differential value competes with the systems noise, a larger DynR and consequently larger differential value is more beneficial for unmixing from a practical standpoint, given that averaging to reduce noise also extends the measurement time. As such, the comparison of the relative DynR of the protein expressing samples with the difference between the highest and lowest blood SNR allows to directly estimate the unmixing ability. Once the protein's relative DynR approximately matches the difference of the blood SNRs, unmixing using simple differential methods is not possible anymore.
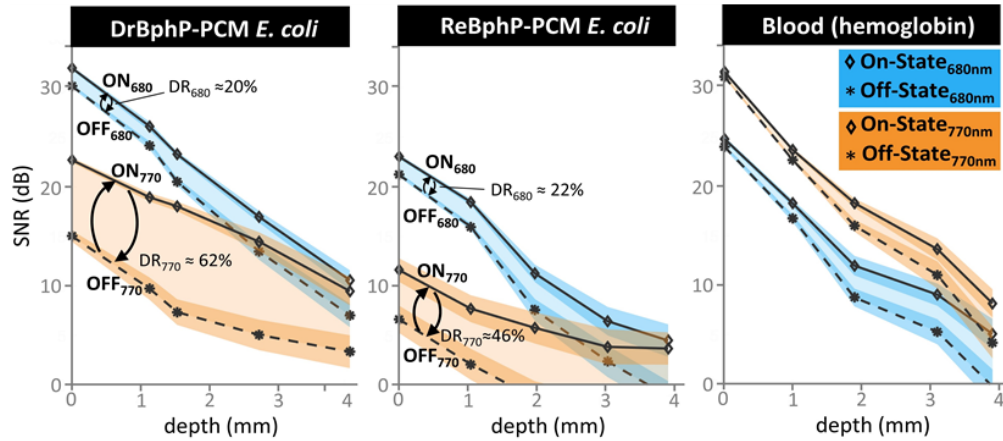

Fig. 3. Signal-to-noise ratio (SNR) in dB of the of the maximum SNR and minimum SNR for DrBphP-PCM and ReBphP-PCM expressing *E. coli* and blood. The maximum SNR is plotted with a solid line and asterisk for 680 nm and with a dashed line and diamonds for 770 nm. For the DrBphP-PCM and ReBphP-PCM expressing *E. coli* the light shaded difference between the maximum and minimum SNR represents the relative dynamic range which is provided also as a percentage for the two protein expressing bacteria cultures. The darker shaded error band represents the estimated remaining standard deviation for each curve.

3.3. Switching kinetics and contrast-to-background ratio

In a last step we evaluated the switching kinetics and the contrast-to-background ratio separately for 680 and 770 nm. In Fig. 4(a) and (b), we show the 680 nm and 770 nm switching curves as well as the exponential curve fittings at a maximum depth of 4 mm for DrBphP-PCM-expressing bacteria and 2 mm for ReBphP-PCM-expressing bacteria. The switching curves tend to elongate and decrease in amplitude at higher depths. As a consequence of dropping amplitude, the switching kinetics for ReBphP-PCM could not be assessed at depths beyond 2 mm. The exponential fittings allowed to access the time constant given in number of pulses, shown in Fig. 4(c), which increases at higher depth as a consequence of the dropping fluence. The overall number of pulses required to switch the proteins is significantly larger when excited with 770 nm compared to 680 nm. The unmixing performance visualized as the contrast-to-background ratio where the blood tubing signal is considered as the background is shown in Fig. 4(d). For cells expressing DrBphP-PCM, the CBR drops from roughly 10.5 to 1.3 at 770 nm and 2.1 to ≈ 1 at 680 nm over a depth of 4 mm. For cells expressing ReBphP-PCM, the CBR drops from roughly 7.8 to 2.4 at 770 nm and 2.1 to 1.1 at 680 nm over a depth of 2 mm. The CBR values approaching 1 indicate, that the system would not be able to differentiate the switching signals of the proteins from the blood signals as noise starts to dominate the signals. Moreover, the CBR values differ greatly between 680 and 770 nm due to the differing DynR.
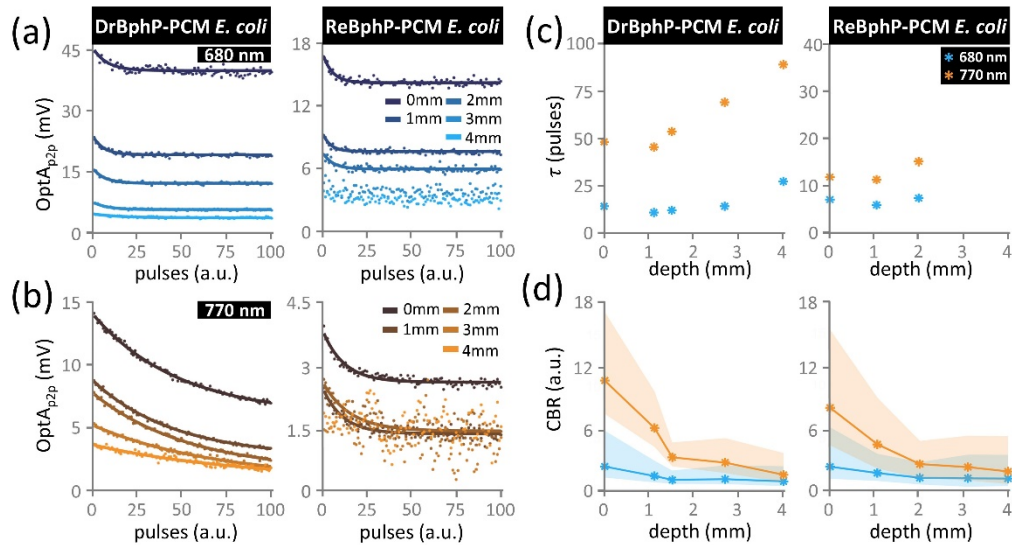
Fig. 4. Switching curves and extracted switching characteristics for the photoswitching proteins (DrBphP-PCM and ReBphP-PCM) expressed by *E. coli*. The proteins' switching curves with exponential curve fittings at a) 680 nm (blue tones) and b) 770 nm (orange tones). c) The relaxation time constants (τ) at different depths extracted from fitting exponential curves to optoacoustic (OptA) signals emitted by DrBphP-PCM- or ReBphP-PCM- expressing *E. coli*. d) The unmixing performance visualized as the contrast-to-background ratio (CBR) at different depths. The shaded error band is the uncertainty range of the CBR due to the remaining standard deviation in both, the bacteria signal and blood signal. Data points at 3 and 4 mm depths for ReBphP-PCM expressing cells are missing in c) due to their lower SNR as a result of lower protein expression, which prevented the analysis.

4. Discussion

The results presented in this study shed light on different aspects such as the SNR and switching kinetics at two different wavelengths of photoswitchable proteins expressed by *E. coli* over various depths using a single-element OptA mesoscopy setup. This includes considerations for the achievable depth and the necessary pulsing schemes to achieve effective switching. Hence, our analysis of the performance of photoswitchable proteins and BphPs in particular, is needed to provide a basis for their integration into single-element detector OptA mesoscopy.

More specifically, we found that the SNR decreased with increasing depth by approximately 5 dB/mm for all samples. This reduction in SNR can be attributed to several factors, including dropping fluence due to light scattering and beam divergence, ultrasound attenuation, and the decreased sensitivity of detectors as the distance from the acoustic focus increases. Our representation of the ON-state and Off-states SNR also allows to directly assess system parameters such as the required SNR improvement to enhance the sensing/imaging depth for example by a protein with higher extinction coefficient, higher expression or increased averaging. Although a scattering phantom has been used, which does not fully reflect the properties of human skin, the significant drop in SNR and assessed DynRs observed are in line with findings from multiple-element transducers and macroscopic implementations [7].

Based on the exponential fitting, the number of pulses required to switch the proteins from the ON- to the OFF-state has been found to greatly increase with depth. For DrBphP-PCM, the number of required pulses almost doubles at a depth of 4 mm depth compared to 0 mm, while for ReBphP-PCM, it increases by roughly a factor of 1.5 at a depth of 2 mm compared to 0 mm.

Moreover, ReBphP-PCM switches 2 to 6 times faster than DrBphP-PCM, which is consistent with previous findings [15,18]. These results provide a basis for establishing a pulsing scheme for the current single-element detector setup, which suggests applying at least 25 pulses at 680 nm or 90 pulses at 770 nm to switch DrBphP-PCM ON and then OFF at a depth of 4 mm. For ReBphP-PCM, the pulsing scheme would require at least 11 pulses at 680 nm and 15 pulses at 770 nm to switch the protein. This comparison of absolute numbers also emphasizes a fundamental difference when assessing switching at two distinct wavelengths as such that depending on the application, switching at different speeds can be utilized even within same protein. Although the switching kinetics in real tissue are expected to differ due to inhomogeneities and absorption, which affect the local fluence, the required pulsing scheme is mainly dictated by the switching kinetics of the proteins. As such, the pulsing scheme serves as a concentration-independent starting point for future integration of photoswitchable proteins in OptA mesoscopy. Moreover, understanding the depth- and thus fluence-dependent switching kinetics could even serve as an estimator of the local fluence in OptA mesoscopy [21].

The unmixing performance expressed as CBR of the two BphPs versus blood drops by approximately a factor of 10 over a distance of 4 mm from the acoustic focus. The unmixing performance at 770 nm is superior for both proteins due to a higher DynR compared to 680 nm, which is in line with previous findings on the extinction coefficient [15,18]. The slightly lower unmixing performance observed for ReBphP-PCM can be attributed to the overall lower SNR due to the lower expression of the protein despite an even higher extinction coefficient and OptA quantum yield [15]. As with the switching kinetics, the two different DynRs within the same protein may be used simultaneously for unmixing depending on the employed wavelength. The overall unmixing performance in this experiment is, similar as for the general evaluation using exponential fittings, limited by the system's noise, causing the CBR to approach a value of 1, which reflects the remaining electrical noise of the system that is equivalent for both the proteins and blood. Another potential compounding factor could be laser fluctuations, which may not be normally distributed and could, therefore, hamper unmixing. Our analysis of the CBR for this experiment further emphasizes the strong dependency on the signal's SNR, providing a benchmark for future studies leveraging OptA mesoscopy with a single-element detector in combination with photoswitchable proteins.

The progress and benefits of photoswitchable proteins are now being analyzed not only in the context of OptA macroscopy with tomographic-like geometries and multi-element detectors but also within single-element detector OptA mesoscopy. The analysis at two different wavelengths enables the extraction of twice as much switching information compared to assessments conducted at a single wavelength. Moreover, analysis at two different wavelengths allows a direct comparison of wavelength-dependent switching dynamics and the associated differences in DynR and SNR. This study provides an initial overview of the expected performance in terms of achievable SNR and detection depth, required pulsing schemes, and unmixing performance in a scattering phantom for single-element OptA mesoscopy. These results are anticipated to accelerate the adoption of photoswitchable proteins in the field of OptA mesoscopy, as the derived pulsing schemes, depth-dependent behavior, and unmixing performance can serve as a starting point for future studies and may even be used to derive new unmixing schemes that take into account the properties of the switching cycles at different wavelength. However, the results cannot be directly transferred to in-vivo measurements due to the more complex structure of real skin. Therefore, the next steps should involve using a more realistic phantom or conducting ex-vivo and in-vivo measurements. Further work is required to address the presented challenges. Low SNR may be mitigated by increasing the optical fluence delivered to deeper layers. The sensitivity of OptA detectors must be increased and/or noise must be decreased. Additionally, faster high-energy lasers must be developed to meet the relatively high total energy requirements for switching

between states of photoswitchable proteins, enabling reasonably high pixel scanning rates and thus enabling actual OptA imaging in the mesoscopic domain.

In summary, we have investigated the use of photoswitchable BphPs in single-element detector OptA mesoscopy at different depths in a scattering phantom. Based on the switching kinetics, we found that the number of pulses required to switch the proteins between the ON- and OFF-states needs to be increased by up to a factor of approximately 2 at a depth of 4 mm. Furthermore, we found that SNR decreases by approximately 5 dB per mm, which limited unmixing to depths of 2 to 4 mm in the current setup. Our experiments reveal the required pulsing schemes, achievable depths, and unmixing performance when using photoswitchable BphPs in OptA mesoscopy. These findings could potentially accelerate the adoption of these proteins in the field of OptA mesoscopy.

Disclosures. V.N. is a founder and equity owner of Maurus OY, sThesis GmbH, iThera Medical GmbH, Spear UG, and I3 Inc. The remaining authors declare no conflict of interest.

Data Availability. Data underlying the results presented in this paper are not publicly available at this time but may be obtained from the authors upon reasonable request.

References

1. L. V. Wang and S. Hu, "Photoacoustic tomography: In vivo imaging from organelles to organs," Science **335**(6075), 1458–1462 (2012).
2. V. Ntziachristos, "Addressing unmet clinical need with optoacoustic imaging," Nat. Rev. Bioeng. **3**(3), 182–184 (2024).
3. F. Knieling, S. Lee, and V. Ntziachristos, "A primer on current status and future opportunities of clinical optoacoustic imaging," npj Imaging **3**(1), 4 (2025).
4. L. Englert, D. Jüstel, and V. Ntziachristos, "The need for optoacoustic microscopy," Rev. Mod. Phys. **97**(1), 015005 (2025).
5. A. C. Stiel and V. Ntziachristos, "Controlling the sound of light: photoswitching optoacoustic imaging," Nat. Methods **21**(11), 1996–2007 (2024).
6. K. Mishra, J. P. Fuenzalida-Werner, F. Pennacchietti, *et al.*, "Genetically encoded photo-switchable molecular sensors for optoacoustic and super-resolution imaging," Nat. Biotechnol. **40**(4), 598–605 (2022).
7. J. Yao, A. A. Kaberniuk, L. Li, *et al.*, "Multiscale photoacoustic tomography using reversibly switchable bacterial phytochrome as a near-infrared photochromic probe," Nat. Methods **13**(1), 67–73 (2016).
8. J. Weber, P. C. Beard, and S. E. Bohndiek, "Contrast agents for molecular photoacoustic imaging," Nat. Methods **13**(8), 639–650 (2016).
9. M. Omar, J. Aguirre, and V. Ntziachristos, "Optoacoustic mesoscopy for biomedicine," Nat. Biomed. Eng. **3**(5), 354–370 (2019).
10. J. Aguirre, M. Schwarz, N. Garzorz, *et al.*, "Precision assessment of label-free psoriasis biomarkers with ultra-broadband optoacoustic mesoscopy," Nat. Biomed. Eng. **1**(5), 0068 (2017).
11. J. Märk, H. Dortay, A. Wagener, *et al.*, "Dual-wavelength 3D photoacoustic imaging of mammalian cells using a photoswitchable phytochrome reporter protein," Commun. Phys. **1**(1), 3 (2018).
12. W. Xia, D. Piras, J. C. G. Van Hespen, *et al.*, "An optimized ultrasound detector for photoacoustic breast tomography," Med. Phys. **40**(3), 032901 (2013).
13. J. Benavides Lara, R. Prakash, and K. Avanaki, "Assessment of a Single-Element Scanning System for Enhanced Photoacoustic Imaging of Brain Hemorrhage," J. Biophotonics **18**(3), e202400153 (2025).
14. B. Yan, B. Song, G. Mu, *et al.*, "Compressed single-shot 3D photoacoustic imaging with a single-element transducer," Photoacoustics **34**, 100570 (2023).
15. L. Li, A. A. Shemetov, M. Baloban, *et al.*, "Small near-infrared photochromic protein for photoacoustic multi-contrast imaging and detection of protein interactions in vivo," Nat. Commun. **9**(1), 2734 (2018).
16. R. Gao, F. Liu, W. Liu, *et al.*, "Background-suppressed tumor-targeted photoacoustic imaging using bacterial carriers, Proc," Proc. Natl. Acad. Sci. U. S. A. **119**(8), e2121982119 (2022).
17. S. Chen, K. Li, X. Chen, *et al.*, "Reversibly photoswitchable protein assemblies with collagen affinity for in vivo photoacoustic imaging of tumors," Sci. Adv. **10**(35), eadn8274 (2024).
18. K. Mishra, M. Stankevych, J. P. Fuenzalida-Werner, *et al.*, "Multiplexed whole-animal imaging with reversibly switchable optoacoustic proteins," Sci. Adv. **6**(24), 24 (2020).

19. G. S. Filonov, A. Krumholz, J. Xia, *et al.*, "Deep-Tissue Photoacoustic Tomography of a Genetically Encoded Near-Infrared Fluorescent Probe," Angew. Chem., Int. Ed. **51**(6), 1448–1451 (2012).

20. A. C. Stiel, X. L. Deán-Ben, Y. Jiang, *et al.*, "High-contrast imaging of reversibly switchable fluorescent proteins via temporally unmixed multispectral optoacoustic tomography," Opt. Lett. **40**(3), 367 (2015).

21. X. L. Deán-Ben, A. C. Stiel, Y. Jiang, *et al.*, "Light fluence normalization in turbid tissues via temporally unmixed multispectral optoacoustic tomography," Opt. Lett. **40**(20), 4691 (2015).